PROCEEDINGS OF SCIENCE

CII Emission from High-Redshift Quasars As a Signature of Obscured AGNs

Evgenii O. Vasiliev,[a,b,*] **Yuri A. Shchekinov**[a,c] **and Biman B. Nath**[c]

[a] *Lebedev Physical Institute of Russian Academy of Sciences, Leninskiy Ave. 53, Moscow, Russia*

[b] *Institute of Astronomy, Russian Academy of Sciences Pyatnitskaya st. 48, Moscow, Russia*

[c] *Raman Research Institute Sadashivanagar, Bengaluru 560080, Karnataka, India*

E-mail: eustar@mail.ru, yus@asc.rssi.ru, biman@rri.res.in

We study the relation between the luminosities in the CII line at 158μm and in the far infrared (FIR) continuum from quasars observed by *ALMA* at $z \geq 6$ and show that the observed relation is better reproduced with a predominance of radiation from an obscured supermassive black hole than with star formation alone. We found that the locus of points in the "CII/FIR–FIR" plane corresponding to the observed set of quasars could be reproduced in our models with the following types of the central ionizing source: (i) a mildly or slightly obscured SMBH with $M_\bullet \gtrsim 10^8 M_\odot$ and a stellar population with bolometric luminosity $L_* < 3L_\bullet$; (ii) a highly obscured SMBH with $M_\bullet \sim 10^6 - 10^8 M_\odot$ and a massive stellar population with bolometric luminosity $L_* \sim 300 L_\bullet$.

The Multifaceted Universe: Theory and Observations - 2022 (MUTO2022)
23-27 May 2022
SAO RAS, Nizhny Arkhyz, Russia

*Speaker

PoS(MUTO2022)016

1. Introduction

Recent observations of galaxies at redshifts $z > 6$ with the Atacama Large Millimeter Array (ALMA) have found a correlation between the flux in the fine-structure CII 158μm line and the far-infrared (FIR) continuum emission of dust at a rest-frame frequency ~ 2THz [1]. Given the quasar-host nature of the target galaxies, it is interesting to study how the presence of a supermassive black hole (SMBH) can affect the relation between the CII line and FIR luminosities. High values of the latter, $L_{FIR} \gtrsim 10^{12} L_{\odot}$, are thought to be analogous to those of ultra-luminous infrared galaxies (ULIRGs) in the low-redshift Universe [e.g., 2, 3]. However, the [CII]-to-FIR luminosity ratio for this high-z sample of galaxies is several times lower than that of ULIRGs at $z \gtrsim 1$ with similar FIR luminosity, although several ULIRGs at $z < 1$ have similar ratio, but their FIR luminosities are lower [see left panel of Figure 8 in 1]. One can guess therefore whether the galaxies observed by ALMA at $z > 6$ represent high redshift analogs of ULIRGs or have different nature. It is worth mentioning that the target galaxies are, by the selection criterion, very bright in the ultraviolet (UV) range: the absolute magnitude of the rest-frame far-UV continuum is $M_{1450} < -25.25$ mag. Such a high UV continuum can suggest a relatively low optical depth at 1450Å, i.e., this criterion tends to select obscured active galactic nuclei (AGNs). On the other hand, the high FIR fluxes suggest the presence of an enormous amount of dust. Recent observations of a massive quasar at $z \sim 7.54$ indeed demonstrate copious dust in ambient gas [4]. In such conditions one expects that there are numerous mildly and highly obscured quasars. Here we focus on studying the spectral features of obscured quasars, especially on the relation between the CII line and FIR luminosities of such objects, and on evaluating the contributions of starbursts and AGNs in heating the dust and ionizing the carbon in obscured galaxies.

2. Model

In the central region of a host galaxy, there are a supermassive black hole (SMBH) and a stellar bulge. We assume that their cumulative radiation ionizes and heats the surrounding gaseous reservoir. Following [5], the SMBH radiation is supposed to be generated by a slim disc [6] with the Novikov–Thorne spectrum [7] modified by a Comptonised extension up to the energy $E > 1$ keV [see details in 5]. Figure 1 presents an example of such a spectrum depicted by the magenta line. For comparison, we add a blackbody spectrum, which illustrates that both in the infrared (IR) and submillimeter (submm) ranges, the SMBH spectrum looks like thermal radiation with effective temperature depending on the SMBH mass $T_{eff} \sim M^{1.5}$ [5]. An inherent feature of the SMBH spectrum is a powerful high-energy part with $E > 0.1$ keV so that such spectrum is believed to be consistent with a composite SED for radio-quiet AGNs [see, e.g., 8].

The stellar population predominantly emits optical and UV photons, which cannot efficiently heat the surrounding gas. More energetic far-UV and soft X-ray emission can be maintained by young massive stars and low-mass stars evolved through the post-AGB phase. Note that the former produce such emission during about 30 Myr after the beginning of a starburst, whereas the latter commences to work after 120–150 Myr. From this point it is useful to consider two models of spectral energy distribution (SED) based on different star formation history: (i) a single (instantaneous-burst) stellar population (SSP) based on the Padova 2000 stellar evolutionary

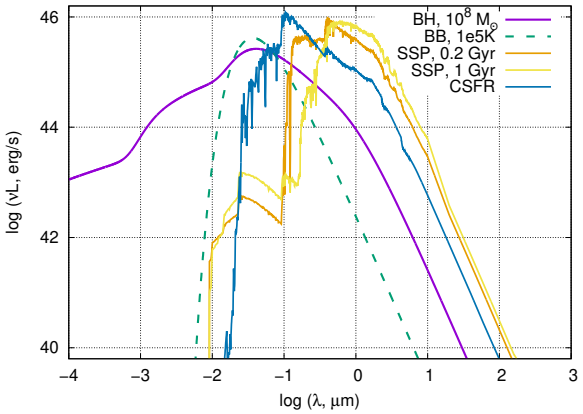

Figure 1: Spectral energy distributions for the models [5] of an SMBH with $M_\bullet = 10^8 M_\odot$ of an Eddington accretion rate (magenta line), for an SSP with ages of 0.2 and 0.9 Gyr (yellow and dark yellow lines) and the bolometric luminosity $L = 3 \times 10^{12} L_\odot$ [9], and for continuous star formation (CSFR) with a constant SF rate $\simeq 10^3 M_\odot \mathrm{yr}^{-1}$ producing a bolometric luminosity $L = 3 \times 10^{12} L_\odot$. The green dashed line shows a BB spectrum with $T = 10^5$ K.

tracks [10] with the Salpeter inital mass function (IMF) [9] and for solar metallicity and (ii) a stellar population being continuously formed (CSFP) with a constant star formation rate obtained using the Starburst99 code [11]. We assume that these two models of stellar populations are inherent to the bulge of the host galaxy.

Figure 1 shows two SEDs of the SSP with ages of 0.2 and 1 Gyr depicted by the dark-yellow and yellow lines. One can clearly find a decrease of near-UV luminosity and a growth of far-UV radiation for the older stellar population. This is due to the transition of more and more low-mass stars to the AGB phase. In case of constant star formation rate, there are multiple stellar populations, so the UV luminosity of young massive stars dominates over that of low-mass AGB stars. Only at the high energy tail (close to the soft X-ray range), the spectrum of the SSP exceeds that of the CSFP. One may guess that this is because of a significant deposit from young massive stars into the total luminosity, which is the same for the considered models and equal to $L = 3 \times 10^{12} L_\odot$. In our calculations the bolometric luminosity of stellar populations are taken from 3×10^9 to $3 \times 10^{12} L_\odot$.

The SMBH and stellar population are surrounded by a gaseous reservoir, which is a source for feeding the black hole and possible further star formation. On one hand, this gas is ionized and heated by the central sources, on the other it may significantly attenuate the SED of these sources at the UV/optical wavelengths. This decrease is determined by the mass of such a reservoir. We consider the gas mass varying from 3×10^8 to $3 \times 10^{10} M_\odot$. These values are consistent both with several observations of AGNs at high redshifts [e.g., 12, 13] and cosmological simulations [see Figure D1 in 14].

Ionization states of various elements and the ionic spectral lines are calculated with the CLOUDY code [15]. The gas is exposed to the cumulative radiation emitted by the central sources, i.e., an SMBH and the stellar population. We assume a spherical geometry, the inner radius of the gaseous shell is fixed at 100 pc, and the outer radius is determined by the gas mass M_g. The density and metallicity are distributed homogeneously. The calculations are made for the SEDs

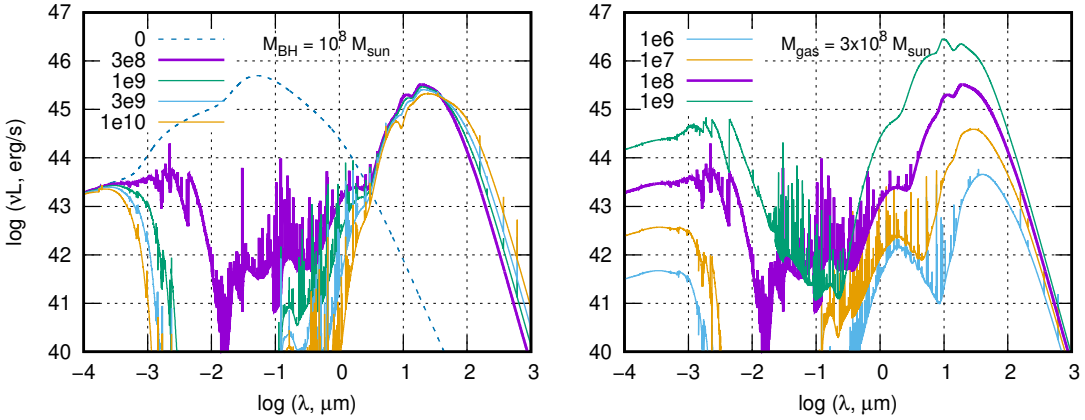

Figure 2: The nebular emission from gas exposed to the stellar population and the black hole. The left panel shows the spectra for gas with masses equal to $3 \times 10^8, 10^9, 3 \times 10^9$, and 10^{10} $M_\odot$, exposed to the stellar population with a bolometric luminosity $L_* = 3 \times 10^9 L_\odot$ and the black hole with a mass $M_\bullet = 10^8$ $M_\odot$. The label "0" corresponds to the unattenuated spectrum from the stellar population and SMBH. The right panel presents the spectra for the gas mass fixed to 3×10^8 $M_\odot$, exposed to the BH with masses $M_\bullet = 10^6, 10^7, 10^8$, and 10^9 $M_\odot$ as indicated in the legend. Gas metallicity is [Z/H] = 0, the dust mass fraction is assumed to be as in the Milky Way, $\mathcal{D} = 0.3\zeta$ (ζ is the metal mass fraction). The stellar population has an age of 0.9 Gyr and solar metallicity.

presented in Figure 1. The fiducial density is $n = 10$ cm^{-3} and the metallicity is set to the solar value [Z/H] = 0. We assume that the gas is in thermal equilibrium.

3. Results

The left panel of Figure 2 presents the nebular emission from gas with masses equal to $3 \times 10^8, 10^9, 3 \times 10^9$, and 10^{10} $M_\odot$, exposed to the stellar population with a bolometric luminosity $L_* = 3 \times 10^9 L_\odot$ and the black hole with a mass $M_\bullet = 10^8$ $M_\odot$. The line labelled by "0" corresponds to the unattenuated spectrum from both the stellar population and SMBH. One can note that the radiation of such a massive BH dominates over the radiation of such a low-luminosity stellar population. To be the deposit of stellar population significant, the luminosity of the population should be higher than $\sim 3 \times 10^4 M_\bullet$ (where $M_\bullet$ is in the solar masses), if a BH accretes with the Eddington rate. However, the stellar populations mainly contribute to the UV/optical range, where the attenuation is quite high, so the stellar deposit can be neglected in the case of such a high mass of a BH. For gas masses higher than $M_g \sim 10^{10} M_\odot$, the SED is almost completely suppressed from X-ray ($\sim$ 1 keV) to IR ($\sim$ 1 μm) wavelengths. A decrease of the gas mass about an order of magnitude leads to less attenuation, but the picture does not change remarkably. For further decrease about three times, i.e., for $M_g \sim 3 \times 10^8 M_\odot$, the optical depth at $\lambda \sim 10^3$Å drops to ~ 7, which leads to significant spectral luminosity in the continuum and numerous lines at rest-frame $\lambda \sim 10^3$Å.

For a fixed gas mass equal to $M_g = 3 \times 10^8 M_\odot$, the increase of the BH mass leads to further ionization of the surrounding gas, so the far-UV luminosity becomes higher, but due to dust the optical luminosity even decreases (the right panel of Figure 2). From this point of view, to get

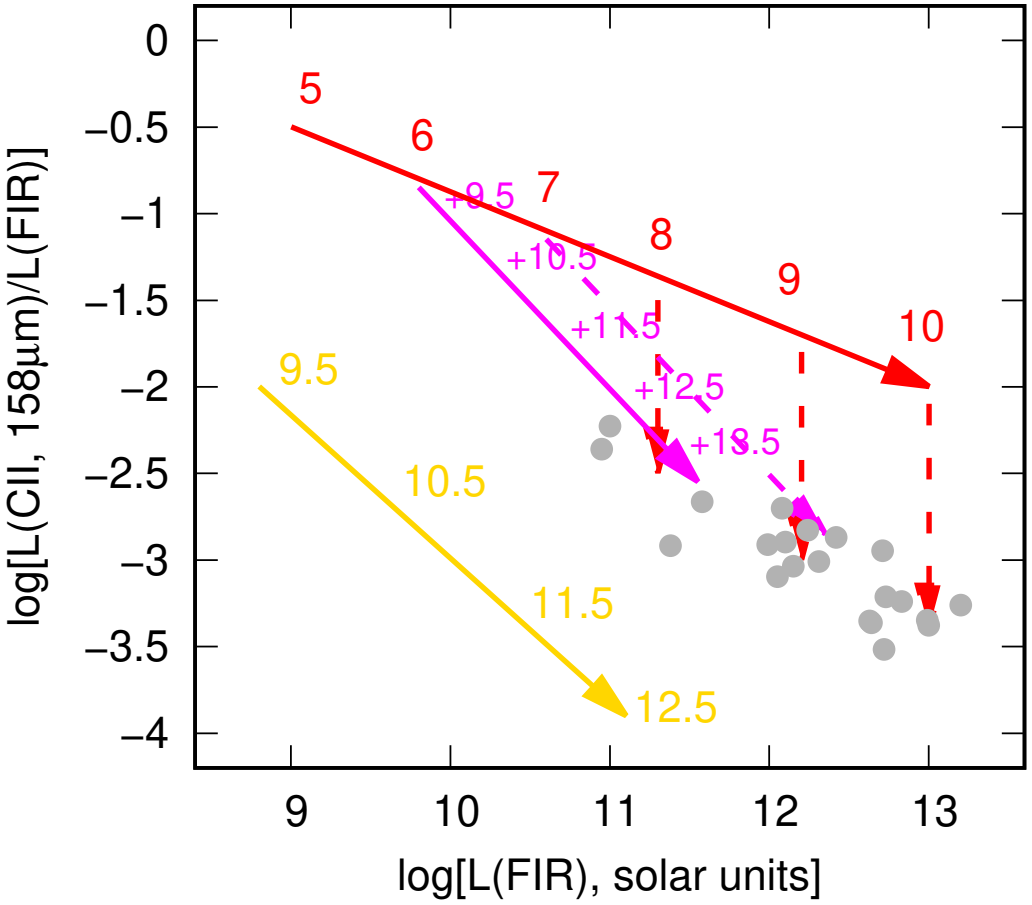

Figure 3: The luminosity ratio of the [CII] 158μm line to the FIR continuum versus the FIR continuum. The small grey circles depict the results from [1, see their Fig. 8]. The FIR continuum is integrated over λ = 42.5–122.5μm. The red solid line corresponds to the models with a highly obscured SMBH without a stellar population. The red labels along the line depict the logarithm of the BH mass. The red dashed lines show how the ratio changes in the models with less obscured SMBHs, i.e., the gas mass decreases along these lines for a fixed SMBH mass (see text for details). The magenta solid line corresponds to the models with a highly obscured SMBH of a mass $M_{BH} = 10^6 M_\odot$ and a stellar population with a constant star formation rate: the magenta labels show the logarithm of stellar luminosity. The magenta dashed line depicts the model of an SMBH with a mass $M_{BH} = 10^7 M_\odot$ and a stellar population. The yellow lines correspond to the models with a stellar population with a constant star formation rate: the labels show the logarithm of stellar luminosity.

sufficiently high luminosity at rest-frame $\lambda \sim 10^3$Å, one should expect high UV/optical luminosity in quite a narrow range of gas mass.

The inclusion of a massive stellar population leads to the increase of luminosity around $\lambda \sim 1\mu$m in the case of bolometric stellar luminosities $L_* \gtrsim 3L_\bullet$, where $L_\bullet$ is the Eddington luminosity of a BH. In the case of lower stellar luminosity, the SED is completely controlled by a BH, and the FIR tail of the nebular emission does not depend on the presence of the stellar population.

Figure 3 presents the luminosity ratio of the [CII] 158μm line to the FIR continuum versus the FIR continuum for several models of spectral energy distributions: (a) only SMBH (without

a stellar population), (b) SMBH and different stellar populations, and (c) only stellar populations. The red solid line corresponds to models with a highly obscured SMBH without a stellar population (the red labels along the line depict the logarithm of the BH mass): the gas mass of a spherical layer surrounding the central SMBH varies from 3×10^8 to $3 \times 10^{10} M_\odot$ depending on the BH mass, which corresponds to high optical depth values $\tau \gtrsim 20$ in the UV/optical range. Such values lead to the BH spectrum suppression from soft X-ray to near-IR wavelengths like fo the spectra with $M_{gas} \gtrsim 10^9 M_\odot$ depicted in the left panel of Figure 2. Low-mass BHs with $M_\bullet \lesssim 10^6 M_\odot$ are completely buried in such a massive gaseous layer. Only a decrease of more than several orders of magnitude of gas mass around a BH with $M_\bullet \lesssim 10^6 M_\odot$ can produce a lower [CII]-to-FIR luminosity ratio. SMBHs with higher masses are more energetic, and the ratio is more sensitive to the gas mass: a decrease of gas mass by 3–10 times around an SMBH of $M_\bullet \sim 10^8 M_\odot$ leads to the drop of the ratio by an order of magnitute, i.e., given such parameters, the point in the "FIR–[CII]/FIR" plane shifts along the red dashed lines for a fixed SMBH mass (Figure 3). Note that this shift is aimed to the locus of the observed data [1].

The inclusion of a stellar population produces an IR excess compared to the SED of a BH (Figure 1), thus for a fixed BH mass the FIR luminosity increases for a more luminous stellar population, whereas the distribution at shorter wavelengths does not change, because it is controlled by a BH. The SED of the stellar population with the bolometric luminosity $L_* \sim 3 \times 10^9 L_\odot$ is close to that of a BH with $M_\bullet \sim 10^6 M_\odot$ at the IR and longer wavelengths. Thus, the point for this model in the "FIR–[CII]/FIR" plane is close to that for the "only BH" model with a BH of $M_\bullet \sim 10^6 M_\odot$ (see the origin of the magenta line in Figure 3, this point is labeled as "+9.5," the symbol "+" reflects that this model includes both an SMBH of $M_\bullet \sim 10^6 M_\odot$ and a stellar population, the number is the logarithm of bolometric stellar luminosity). One can see that an increase of stellar luminosity leads to a shift in the "FIR–[CII]/FIR" plane along the magenta solid line. The model corresponding to the enormous luminosity of greater than $3 \times 10^{12} L_\odot$ is close to the locus of the observed points. For higher masses of the BH, the line can be shifted parallel, but the stellar luminosity value at the intersection with the red line increases as $L_*^i \sim M_\bullet$. For instance, the magenta dashed line depicts the models with an SMBH of a mass $M_{BH} = 10^7 M_\odot$ and a stellar population. Given such conditions, one can approach to the upper border of the observed data locus. Note that in these models the gas mass is kept at high values, so such SMBHs are highly obscured, their AB magnitude is large (the UV luminosity is low), therefore such objects have not been selected as targets in the survey [1] (to be remembered, the target galaxies in the sample obtained in [1] have small M_{1450}).

Let us consider the stellar population as the only central source. Due to low luminosity in far-UV/X-rays (see Figure 1), the stellar population does not efficiently ionize and heat surrounding gas. Then, one should significantly decrease the mass of the gaseous layer to get the thermal equilibrium, e.g., it is down to $M_{gas} \sim 3 \times 10^7 M_\odot$ for $L_* \sim 3 \times 10^9 L_\odot$. However, a set of models for several stellar luminosities has been calculated. The yellow line corresponds to the models for the stellar population with a constant star formation rate (CSFP): the labels show the logarithm of stellar luminosity. An increase of gas mass shifts the line to higher values of the ratio. One can note that the absence of a BH leads to a dramatic change of the locus in the "FIR–[CII]/FIR" plane, which is far from the observed data. Moreover, in these models the gas mass is quite low in comparison with the stellar luminosity.

4. Conclusions

Our results are summarized as follows:

- the observed [CII]-to-FIR luminosity ratio for $z > 6$ AGNs [1] is better reproduced with a predominance of radiation from an obscured SMBH than with star formation alone;
- the locus of points in the "CII/FIR–FIR" plane corresponding to the observed AGNs [1] could be reproduced in our models with the following types of the central ionizing source: (i) a mildly or slightly obscured SMBH with $M_\bullet \gtrsim 10^8 M_\odot$ and a stellar population with the bolometric luminosity $L_* < 3L_\bullet$; (ii) a highly obscured SMBH with $M_\bullet \sim 10^6 - 10^8 M_\odot$ and a massive stellar population with a bolometric luminosity $L_* \sim 300 L_\bullet$.

Acknowledgments

The work of YS was partially supported from the project "New Scientific Groups LPI," 41-2020. EV is thankful to the Russian Scientific Foundation (grant 19-72-20089).

References

[1] R. Decarli, F. Walter, B.P. Venemans, E. Bañados, F. Bertoldi, C. Carilli et al., *An ALMA [C II] Survey of 27 Quasars at z > 5.94*, *Astrophys. J.* **854** (2018) 97 [1801.02641].

[2] D. Farrah, V. Lebouteiller, H.W.W. Spoon, J. Bernard-Salas, C. Pearson, D. Rigopoulou et al., *Far-infrared Fine-structure Line Diagnostics of Ultraluminous Infrared Galaxies*, *Astrophys. J.* **776** (2013) 38 [1308.4165].

[3] K.L. Larson, D.B. Sanders, J.E. Barnes, C.M. Ishida, A.S. Evans, V. U et al., *Morphology and Molecular Gas Fractions of Local Luminous Infrared Galaxies as a Function of Infrared Luminosity and Merger Stage*, *Astrophys. J.* **825** (2016) 128 [1605.05417].

[4] B.P. Venemans, F. Walter, R. Decarli, E. Bañados, C. Carilli, J.M. Winters et al., *Copious Amounts of Dust and Gas in a z = 7.5 Quasar Host Galaxy*, *Astrophys. J. (Letters)* **851** (2017) L8 [1712.01886].

[5] A. Kubota and C. Done, *A physical model of the broad-band continuum of AGN and its implications for the UV/X relation and optical variability*, *Monthly Notices Royal Astron. Soc.* **480** (2018) 1247 [1804.00171].

[6] M.A. Abramowicz, B. Czerny, J.P. Lasota and E. Szuszkiewicz, *Slim Accretion Disks*, *Astrophys. J.* **332** (1988) 646.

[7] I.D. Novikov and K.S. Thorne, *Astrophysics of black holes.*, *Black Holes (Les Astres Occlus)* (1973) 343.

[8] L.C. Ho, *Nuclear activity in nearby galaxies.*, *Annual Rev. Astron. Astrophys.* **46** (2008) 475 [0803.2268].

[9] G. Bruzual and S. Charlot, *Stellar population synthesis at the resolution of 2003*, *Monthly Notices Royal Astron. Soc.* **344** (2003) 1000 [astro-ph/0309134].

[10] L. Girardi, A. Bressan, G. Bertelli and C. Chiosi, *Evolutionary tracks and isochrones for low- and intermediate-mass stars: From 0.15 to 7 M_{sun}, and from Z=0.0004 to 0.03*, *Astron. and Astrophys. Suppl.* **141** (2000) 371 [astro-ph/9910164].

[11] C. Leitherer, D. Schaerer, J.D. Goldader, R.M.G. Delgado, C. Robert, D.F. Kune et al., *Starburst99: Synthesis Models for Galaxies with Active Star Formation*, *Astrophys. J. Suppl.* **123** (1999) 3 [astro-ph/9902334].

[12] B.P. Venemans, F. Walter, R. Decarli, E. Bañados, J. Hodge, P. Hewett et al., *The Compact, ~1 kpc Host Galaxy of a Quasar at a Redshift of 7.1*, *Astrophys. J.* **837** (2017) 146 [1702.03852].

[13] B.P. Venemans, F. Walter, R. Decarli, C. Ferkinhoff, A. Weiß, J.R. Findlay et al., *Molecular Gas in Three $z \sim 7$ Quasar Host Galaxies*, *Astrophys. J.* **845** (2017) 154 [1707.05238].

[14] M. Habouzit, Y. Li, R.S. Somerville, S. Genel, A. Pillepich, M. Volonteri et al., *Supermassive black holes in cosmological simulations I: M_{BH} - $M_\star$ relation and black hole mass function*, *Monthly Notices Royal Astron. Soc.* **503** (2021) 1940 [2006.10094].

[15] G.J. Ferland, M. Chatzikos, F. Guzmán, M.L. Lykins, P.A.M. van Hoof, R.J.R. Williams et al., *The 2017 Release Cloudy*, *Revista Mexicana Astronom. Astrofís.* **53** (2017) 385 [1705.10877].